Impact of Cellular Geometry on Nuclear Dynamics

A thesis submitted towards partial fulfillment of

5 year Integrated BS-MS programme

by

Madhuresh Sumit

Under the guidance of

G V Shivashankar

Associate Professor, Mechanobiology Institute

National University of Singapore, Singapore

IISER Mentor:

Aurnab Ghose

Assistant Professor, Department of Biological Sciences,

Indian Institute of Science Education and Research, Pune

NUS National University of Singapore | MBI MECHANOBIOLOGY INSTITUTE Singapore

Certificate

This is to certify that this dissertation entitled "Impact of Cellular Geometry on Nuclear Dynamics" towards the partial fulfillment of the 5 year integrated BS-MS programme at the Indian Institute of Science Education and Research Pune, represents original research carried out by Madhuresh Sumit at Mechanobiology Institute, National University of Singapore, Singapore under the supervision of G V Shivashankar, Associate Professor, Mechanobiology Institute and Department of Biological Sciences, National University of Singapore, Singapore.

Supervisor

Date: 04/06/2011

Place: Singapore

Head of the Department

Date:

Place:

MECHANOBIOLOGY INSTITUTE, Singapore
National University of Singapore
T-Lab, #05-01
5A Engineering Drive 1
Singapore 117411
FAX : (65) 6872 6123
EMAIL : mbi@nus.edu.sg

COMPANY REGISTRATION NO.: 200604346E

Title Page

Title: Impact of Cellular Geometry on Nuclear Dynamics

Author Affiliations:

Madhuresh Sumit[1] & G V Shivashankar[2]

[1]Indian Institute of Science Education and Research, Homi Bhabha Road, Pashan, Pune 411008, India

[2]Mechanobiology Institute and Department of Biological Sciences, Engineering Drive 1, National University of Singapore, Singapore

Corresponding Author:

Madhuresh Sumit

Indian Institute of Science Education and Research, Homi Bhabha Road, Pashan, Pune 411008, India

Keywords: cell shape, nuclear rotation, micro-contact printing, acto-myosin, dynein

Abbreviations: μCP – micro-contact printing; PDMS - Poly-dimethylsiloxane; EHNA - Erythro-9-(2-hydroxy-3-nonyl) adenine

ABSTRACT

Nuclear movement or dynamics is required for various physiological functions including migration, mitosis, polarization and fertilization. Recent experiments have revealed that different cytoskeletal components and molecular motors are involved in nuclear movement when cell is exposed to different external stresses like shear stress, stretching or wound healing. However, the mechanism of nuclear movement in a stationary cell under normal physiological conditions still remains unclear. In this work, we first observe and characterize the role of cell shape on nuclear dynamics and further investigate the role of cytoskeletal proteins and its associated motors to determine the mechanism involved. Using the fibronectin coated micropatterned substrate of various geometry, we could confine the cells to a particular area and engineer its shape: symmetrical and asymmetrical. Our findings indicate that the cell shape indeed affects the nuclear movement, as characterized by its rotation and translocation dynamics. Further, using drugs for inhibition of acto-myosin contractility and dynein motor we find that nuclear rotation is a consequence of active cytoskeleton around the nucleus.

Keywords: cell shape, nuclear rotation, micro-contact printing, acto-myosin, dynein

INTRODUCTION

Proper localization of nucleus in a eukaryotic cell has been shown to play a very crucial role in many cellular functions such as migration, mitosis, polarization, fertilization and other physiological functions (1-2). Based on our current understanding of the internal cellular architecture, the nucleus cannot be considered as a passive body anymore during these dynamic processes. Nucleus and the cytoskeletal components in the cell have been shown to use the internal tensegrity in order to actively control the physiological processes (3-4). Also during cell migration, the nucleus translocates in a very specific manner, coupled with enhanced nuclear rotation while the centrosome remains almost stationary, positioned between the nucleus and the leading edge of migration (5). The golgi complex displaces from its juxta-nuclear position and localizes to a rearward position (6). Nuclear movements have mainly been attributed to be microtubule dependent involving microtubule polymerization dynamics, Microtubule Associated Proteins (MAPs), motor proteins and cortical anchors (7). However, the involvement of all the three cytoskeletal components- actin filaments, microtubules and intermediate filaments to specific extents in different cell types has also been speculated (1). Moreover recently, linear arrays of nuclear membrane proteins termed as TAN lines, have been shown to utilize the retrograde actin flow in order to control nuclear movements (8). Imposing external physical stresses have also been shown to alter the nuclear movements inside the cell. External shear stress has been shown to enhance the rigid body movements of the nucleus leading to an increase in the nucleus translocation and a significant increase in concerted nuclear rotation (9). In yet another experiment, it has been shown that employing equi-biaxial stretching on a cell leads to nuclear rotation in one direction, while the direction of rotation changes when the membrane is relaxed without complete reversal of the nuclear position (10).

Various nuclear as well as cytoskeletal components play crucial roles in such nuclear dynamics. Nuclear membrane proteins viz. SUN and KASH proteins are involved in transferring forces generated in the cytoplasm to the nuclear core during nuclear movements in the event of migration, mitosis, telomere clustering and intermediate filament association (11). SUN and KASH proteins, together named the LINC Complex connect the cytoskeleton to nucleo-skeleton. Nesprin 2G, an outer nuclear membrane protein, physically interacts with cytoplasmic actin through its actin binding domain while it is connected to the nucleoskeleton through SUN1 and SUN2 proteins, present in the inner nuclear membrane (12). SUN1 is shown to interact with Lamin A inside the nucleus and with Nesprin on the other side and hence establishes a physical connection between nucleus and cytoskeleton (13). The LINC complex also couples the nuclear heterochromatin with the cytoplasmic microtubules mechanically through various protein interactions (14). Actin cables have been shown to be coupled with the nuclear membrane through specific membrane proteins belonging to the LINC complex during nuclear movements indicating actin dependent force transductions (8). The nucleus-cytoskeleton connection plays a significant role in mechanical regulation of the nucleus. Depolymerization of various cytoskeletal components and inhibition of myosin and kinesin motors have been shown to alter the nuclear shape and size (15).

Although research in this field in past a few years has revealed some understanding of the molecules involved in nucleo-cytoskeletal connections and also how the connections are established, the mechanism for nuclear movements in the cellular microenvironment is still little known. More particularly, the components involved in nuclear rotation under different physical

stress conditions have been found to be entirely different. Whereas cells subjected to cyclic strain undergo actin-dependent nuclear rotation without any significant involvement of microtubules (10), shear stress leads to a microtubule dependent rotation without any significant involvement of actin (9). Nuclear rotation during cell migration has been shown to be MT dependent and involves active participation of dynein motors (5). MT dependent dynein motor mechanism has been further supported by a torque-based theoretical model of dynamic instability (16).

The contradictory results in the literature motivated us to ask how actually nuclear movement and rotation inside a stationary cell takes place and which of the cytoskeletal components are primarily involved in nuclear dynamics in a stationary cell which is not subjected to any external physical stress. The approach taken in this work is to use microfabricated patterns in order to confine cells to different geometries and also to manipulate the cytoskeletal symmetry of a cell so as to understand how it affects the nuclear dynamics. We also investigated the role of individual cytoskeletal component and molecular motors in the inherent dynamics using drug inhibitions and plasmid transfections. Proper understanding of the mechanism will give us an idea how the dynamics is regulated inherently in a cell. Consequently, it will enable us to tune the dynamic cytoskeletal-nuclear interaction in order to bring about controlled mechanotransduction.

MATERIALS AND METHODS

Preparation of PDMS Stamps for cell patterning

Poly-dimethylsiloxane (PDMS) stamps were prepared from PDMS Elastomer (SYLGARD 184, DOW Corning) and the ratio of curer to precursor used was 1:10. The curer and precursor were mixed to homogeneity and poured onto the micro-patterned silicon wafer. Prior to this addition, the wafers were properly washed and sonicated with Isopropanol for 20 minutes, dried over nitrogen gas and the surface was silanized with Trichloro (1H, 1H, 2H, 2H- perfluoro-octyl) silane (Sigma Aldrich,) in a desiccators. The wafer with PDMS-crosslinker mix was then degassed under low pressure at 15mbar for around 30 minutes to remove any trapped air bubbles. Then the PDMS-mix on the silicon wafer was baked at 80°C for 2 hours (See Supplementary Figure S3 for illustration of Casting protocol). Finally, the stamps were peeled off from the silicon wafer and used for micro-contact printing (stamping) of fibronectin on hydrophobic dishes.

Labeling of Fibronectin with various dye molecules

Fibronectin protein was labeled using Alexa Fluor Protein Labeling Kit (Invitrogen). Fibronectin (Sigma Aldrich) was first diluted to a concentration less than 2 mg/mL in PBS. Then following the protocol specific for different dye molecules, the mix was stirred at Room Temperature for 1 h. This was followed by further purification and dialysis. The working solution of fibronectin for stamping purpose was prepared by taking 5 % labeled and 5 % unlabeled fibronectin in PBS/Water. The working solution was stored at 4 °C.

Stamping of Fluorescent Fibronectin

Micro-patterned PDMS stamps were oxidized and sterilized under high power in Plasma Cleaner (Model PDC-002, Harrick Scientific Corp) for 5 minutes. 30µl of 50µg/ml fibronectin solution (prepared by mixing 27.3µl of 1xPBS to 1.5µg of 1mg/ml fibronectin and 1.2 µl of fluorescence dye) was allowed to adsorb onto the surface of each PDMS stamp under sterile condition and shielded from light for around 10 minutes till the surface was almost dry. The PDMS stamp was then carefully deposited onto the surface of the non tissue culture plastic bottom petri-dish (1.5 mm thickness for High-resolution imaging) or Iwaki hydrophobic non-treated dish (For Phase contrast imaging) to allow the transfer of the fibronectin micro-features. Subsequently, stamped petri dishes were inspected under fluorescent microscope to verify the smooth transfer of fibronectin micro-patterns. Surface of sample was then treated to passivate non-fibronectin coated regions by 1ml of 2mg/ml Pluronic F-127 for 2 hours.

Cell Culture

NIH 3T3 fibroblasts (ATCC) were cultured in DMEM (Invitrogen) containing 10% Fetal Bovine Serum (GIBCO Invitrogen,) and 1% Penicillin-Streptomycin (Invitrogen). Cells were maintained at 37°C in a 5% CO_2/ 95% air incubator in humidified conditions. Around 60,000 cells were seeded on each time on patterned surfaces (with 10,000 patterns) for 30 minutes, after which the floating/unattached cells were removed and fresh media was added in the dishes. For culture purpose and plasmid transfection, Nunc glass bottom dishes were used. For confocal imaging, low well non-treated hydrophobic dishes (ibidi) were used. For Phase contrast microscopy, Iwaki 35mm non-treated dishes were used.

Plasmid Transfection

Transfection of various plasmids in NIH 3T3 cells was carried out using Lipofectamine 2000 (Invitrogen). 500-1000ng of plasmid and 5 µl of Lipofectamine 2000 were mixed separately in eppendorf containing 100 µl of OptiMEM (serum free media). Lipofectamine mix was centrifuged for 30 sec and was then added to optimum containing plasmid. The final mixture was incubated for 30-40 minutes and then final volume was made to 1ml before adding drop by drop to 50% - 60% confluent culture which was washed with OptiMEM to remove all the serum. After incubation for 3 hours, 1.0 -1.5 ml of normal cell culture media (DMEM with 10% FBS) was added and left for incubation for 18 h. The transfected cells were then trypsinized and seeded on patterned *ibidi* dishes for confocal imaging.

Drug Treatment

Drugs were added after the cells had been seeded and well spread on the micro-patterned dishes. Prior to drug addition, the normal media was removed from the dishes and then 2 ml of fresh media containing the drug was added. The drug concentrations used were as follows: nocodazole: 0.25µg/ml (for depolymerization of microtubules), blebbistatin: 1.25 µM (For inhibition of myosin II), Erythro-9-(2-hydroxy-3-nonly) adenine (EHNA): for inhibition of dynein)

Phase Contrast and Confocal Imaging

Phase Contrast imaging of cells seeded on different geometrical patterns (with or without drug treatment) was done on Nikon Biostation IMQ at 40X air objective (0.5 NA, with correction ring). Time lapse images were acquired at the interval of 5 minutes for 12 h on 1.3 megapixel high sensitivity monochrome camera (1290 X 800, 16-bit images). For confocal imaging of triangular cells transfected with various plasmids (Lifeact-EGFP and EB1-EGFP), Olympus IX81 Inverted Microscope (100X, iol-immersion objective, 1.4 NA) equipped with Perkin Elmer spinning disk confocal system was used. Confocal images were acquired on C9100-13 EMCCD camera (512x512 pixels, back-illuminated). EGFP and GFP tagged proteins were excited with 488 nm laser (Laser type DPSS, 4% - 9 % laser, maximum power 50mW) and the emission was collected with a 527 nm – 555 nm bandpass filter.

Image and Statistical Analysis

Image processing of phase contrast images was done using ImageJ (public domain software developed at National Institutes of Health, Bethesda, MD, USA). Tracking of nucleoli was done using the plug-in MtrackJ (Biomedical Imaging Group, Rotterdam). LabVIEW (National Instruments, Austin, TX, USA) was used to write programs for analysis of the dynamics. Other statistical analysis and graph plotting was done using ORIGIN 8 (Originlab, Northampton, MA, USA). To analyze the dynamics, we considered nucleus as a rigid body. Since very few nuclei undergo wobbling in z-direction, we could simplify the dynamics in two components viz. two-dimensional translational motion and rotation with axis in z-direction. Translational coordinates (centroid position of the nuclei) is given by $(x_{trans}, y_{trans}) = (\frac{x1+x2}{2}, \frac{y1+y2}{2})$ where (x1, y1) and (x2, y2) are the coordinates of two diagonally opposite nucleoli at a given time-point 't' (Figure 1B ii) The slope of the line formed between the centroid and one of the nucleoli is given by $\tan\theta = \left(\frac{y1-ytrans}{x1-xtrans}\right)$.

RESULTS

Micro-contact printing (μCP) of labeled-fibronectin using PDMS stamps

In order to constrain cells on various geometrical shapes, it is of primary importance that we create proper micro-patterns of fibronectin reproducibly. Our goal to understand the nuclear dynamics requires that we observe a large number of cells on patterned substrate in order to analyze them with statistical significance. Although the micro-contact printing (μCP) technique has been extensively used for cell-patterning, proper two-dimensional arrays of micro-patterns requires optimization of the various factors and conditions. Poly-(dimethylsiloxanes) or PDMS is a hydrophobic polymer material. Since polymer materials usually have low surface tension, proper spreading of a polar liquid (for example, fibronectin in PBS buffer) is not achieved due to its hydrophobic surface. In this context, plasma modification of polymer surfaces has been devised using RF-plasma of gas discharge (17-18). Treatment with different gases for plasma has been shown to change the contact angle to different extent. Oxygen (O_2) is a chemically active gas which leads to formation of functional groups such as -OH, -OOH etc. Since the labeled fibronectin solution is prepared in Phosphate Buffer Saline (PBS), proper treatment of PDMS stamps with oxygen-plasma is required to increase the surface tension of the stamp and facilitate proper spreading of the solution. However, extensive plasma treatment also leads to a highly hydrophilic surface and hence transfer of the fibronectin solution to the dishes becomes difficult. Therefore, optimization of the conditions for (μCP) becomes an important step for our study. Another factor that is crucial is the 'drying time' during which the grooves in the micro-pattern get dried of the fibronectin solution. If the stamp is less dry, it leads to patchy patterns, whereas a more dried stamp leads to improper transfer of fibronectin.

Initial trials of fibronectin-μCP to create micro-patterns of fibronectin labeled with Alexa-546 are shown in Figure 1. Patterns having holes and look over-dried could be easily observed. This happens either due to the improper or less plasma treatment of the PDMS stamps or because of the over-drying of fibronectin solution before transfer or stamping. Both these factors can be optimized by variation and fine-tuning. We also find that the drying time and change in hydrophilicity due to plasma treatment depends upon the size of the patterns. Smaller grooves dry faster and vice versa. Thus, for a PDMS stamp peeled off from a particular silicon wafer, the conditions for proper transfer should always be optimized. Figure 1B shows micro-patterns which have been transferred properly. In contrast to the micro-patterns in Figure 1A, these patterns do not show any holes and over-flown patches. However, in some part of the figure, we find that there are faint patterns with patches or holes in them adjacent to the properly transferred patterns. This happens when the stamps move or shake a bit during stamping. So proper care is required during the pattern transfer/stamping process. Once all the above factors have been fine tuned, we get micro-patterns of proper shapes, perfectly homogenous and properly transferred as shown in Figure 1 C. The efficiency of getting such homogenous and properly transferred patterns however varies. To check the homogeneity of the patterns, we measured the intensity profile of the image drawing a straight line through the micro-patterns. The profile indicates that the transfer is almost homogenous varying only in the range of (+/-) 5% as shown in Figure 1D. The sharp features of the curve indicate that fibronectin has been transferred without leaking outside the geometric boundary. Once the conditions for micro patterning have been optimized, we cells need to be seeded on the patterns. In this context, the density of cells to be seeded also needs to be optimized in order to get single cell on the micro-pattern. In the next section, we

investigated what should be the optimum value for cell density so that we get maximum number of single cells.

Cell density optimization for seeding on micropatterns

In order to investigate the dynamics of the nucleus, it is important that we observe as many cells as possible on the micro-patterns so as to make conclusions with statistical significance. In the previous section, we have already shown that a two-dimensional array of micro-patterns cab be created by optimizing and fine-tuning various factors. The next task in our experimental strategy is to seed single cells on these micro-patterns. When we seed a few cells on these patterns, they randomly pick any of the micro-pattern and spread there. This definitely gives single cells on patterns. On contrary, when the density is very high, the probability that more than one cells pick the same micro-pattern increases. Consequently, we find two or three and sometimes four cells sitting on the same pattern. However, this does not serve the purpose of our experiment because two cells sitting on a square pattern are more likely to assume two right triangular shapes. Two cells on a circular pattern lead to two semi-circular cell shapes. Moreover, the cell surface area is also reduced because the same micro-pattern area is shared by two or more cells. So we varied the cell density while seeding so as to find the optimum value for maximum single cells on a given pattern.

Cells were observed on fibronectin patterns once they have spread and taken proper shape Figure as shown in Figure 2A. Although many cells are single on each of the micro-pattern, we can see that there are a few sites where two cells are competing for the same space. Some of the micro-patterns remain unoccupied as well. Figure 2B is a demonstration of single or multiple cells adhering at the same site for circular, square and triangular patterns. Clearly, when multiple cells adhere on the same micro-pattern, they still confine themselves in the same patterned area and compete for the space. Sometimes this competition leads a highly dynamic state of the competing cells where each one crosses the other in order to find some more space (Supplementary Movie 1). In order to understand nuclear dynamics, we chose to track only those cells which are single on the patterns. So, it was necessary to get maximum number of cells which are singly occupied.

The optimization was done by taking different cell densities and seeding the cells on the micro-patterns. This was followed by incubation for around 20 – 30 minutes so that cells start occupying the micro-patterned sites after which, the remaining cells which were still floating were sucked out and media was replaced. Figure 2 C is a plot of percentage of single cells versus the cell density. We found that at around 60,000 cells per dish, the number of single cells occupying single sites is better than other cell densities. Densities lower than this lead to increasing number of unoccupied sites. On the other hand, densities higher than this (60,000 per dish) lead to more number of sites with two or more cells. In the experiments that follow, we have used cell density of around 60,000. It is noticeable that the number of patterns in a single silica wafer varies depending upon the design requirements. So, the cell density needs to be optimized for each PDMS pattern. Once, we established the optimum cell density, we investigated the dynamics of nuclei on these cellular shapes, as described in the next sections.

Nuclear dynamics of NIH 3T3 cells on patterned substrate

Nucleus is connected to different cytoskeletal components in a cell and cytoskeleton provides shapes to the cells. In order to understand the mechanism of mechanotransduction properly, one needs to know how these shapes affect the nucleus. One aspect is to understand how these cytoskeletal structures affect the dynamics of the nucleus in a stationary cell not imposed to any external forces like shear stress or stretching. To study such dynamics, cells are required to be fixed in space followed by observing the nuclear dynamics. In order to achieve this, NIH 3T3 cells were confined on various geometrical fibronectin patterns. The schematic for the approach that we have taken in the following experiments is shown in Figure S1 A (See Supplementary Materials, Figure S1). Varying the rotational and translational symmetry of the cell pattern is equivalent to changing the cytoskeletal micro-environment surrounding the nucleus. Triangle (C_3), Square (C_4) and Circle (C_∞) respectively have increasing order of rotational symmetry and hence they provide lesser and lesser rotational hindrance. In order to create translational hindrance around the nucleus, cells were also seeded on rectangular patterns of sides *a* and *b* as length and breadth respectively, where the value of $n = a: b$ was increased from 1 to 5. Such rectangular patterns provide a simple variable for decreasing translational symmetry for a nucleus. Since a typical fibroblast cell spreads to 1200-1400 μm^2, the area of all the geometrical patterns was kept constant about 1600 μm^2 in order to facilitate proper spreading as well as constrain the cell to assume the geometry of the pattern.

Phase Contrast images were taken for NIH 3T3 cells spread on the shape of the fibronectin pattern after seeding (see Supplementary Figure S1 B). Fibroblast cells achieve the shape of the pattern within half an hour of seeding. The centroid of each of two dark spots (representing nucleoli) inside the nucleus was tracked in the time lapse movies using MTrackJ plug-in in ImageJ. The mean of the two positions gave the translational trajectory of the nucleus. A typical trajectory of the nucleoli-pair on a rotationally symmetric and a non-symmetric pattern is shown in Figure 3A. Clearly, it can be inferred from the trajectory that the nucleus is not a stationary body inside the cell even when the cell is stationary and no external stresses are imposed. Rather, the nucleus seems to have an active dynamics and its trajectory spans in similar way as the pattern. The movement of the nucleus is confined according to the geometry of the cell and hence geometrical constrains on the cell imposes similar constrains on the nucleus. Figure 3 B shows the method employed to resolve the nuclear movement into rotational and translational components. Using programming software LabVIEW, the trajectories of the nucleoli were analyzed to get the rotational motion of the nucleus as discussed in the Materials and Methods Section. Figure 3A (inset) shows a typical translational plot of nuclear motion, determined by taking the mean position of the two nucleoli.

Resolving the rotational and the translational trajectories for nuclei as described in the Methods and Materials section, we obtained the multiple trajectory plots for all the rotationally symmetric shapes as shown in Figure 3 C. The first row panel in the figure shows rotational trajectories for circles, squares and triangles respectively. It is clear that stationary cells of different shapes undergo nuclear rotation even when there is no external stress or shear force applied to them. However, the time scale may not be the same which we investigate in further sections. Moreover, the nuclei also have translatory component and the trajectory spans the cell area as shown in the second row panel of Figure 3 C. From the above analysis, we infer that the stationary cell nuclei rotate as well as translocate. The nucleus has been shown to be actively connected to various cytoskeletal components (8, 11-15). To investigate whether these cytoskeletal components have a role in such nuclear dynamics, different cell shapes provide a convenient variable. Cells on

different geometrical shapes have different cytoskeletal organization (data not shown). Any change in the microenvironment of the nucleus due to cytoskeletal organization should reflect in the dynamics. To investigate whether the cell shape (and hence the cytoskeletal organization) affects this dynamics, we further analysed the rotational trajectories of the nuclei for different rotational geometries as described in the next section.

Nuclear Rotation is cell-shape dependent

When the cells are constrained to assume distinct shapes, they are eventually constrained to organize their cytoskeleton accordingly. Hence cell shape indirectly provides a distinct micro environment around the nucleus. To understand how this shape confinement affects the nuclear dynamics, cells on various geometrical fibronectin patterns were observed live at the interval of 5 minutes for 12 hours under Nikon Biostation microscope in Phase contrast mode using 40x air objective. A typical time lapse movie of a triangular cell is shown in Figure 4A. Visualizing the nucleoli position with respect to time (marked with arrow), the nucleus can be inferred to be rotating. Since the cell is confined in the geometrical pattern, it is clear that only the nucleus is rotating and not the entire cell. After tracking the nucleoli and resolving the dynamics into rotational and translational components, the angle versus time graph was plotted for various cells on all the three geometries as shown in Figure 4B (first row panel). The change in angle in every 5 minutes was determined from the curves and histograms were plotted to find the distribution of instantaneous angular velocity. In order to understand the effect of cell shape on angular velocity, the histograms were fitted to an exponential function for each of the geometric shapes as shown in Figure 4B (second row panel).

A typical angle trajectory of a nucleus on triangular pattern is shown in Figure 4C. When we analysed the nuclear rotation dynamics, we found that it typically has these three properties- rotation (a change in the angle with respect to time), reversal (change in the direction of rotation) and stalling (no significant change in angle with respect to time). Although when the nucleus is rotating in one direction, there are always some small fluctuations. However, sometimes the nucleus undergoes complete reversal of the direction of rotation. Apart from that, sometimes (mostly before or after reversal) there is a time gap in which the nucleus stalls i.e., fluctuates rotationally without actually moving in any of the two directions. The change in angle in unit time (per 5 minutes in this analysis) was computed for 20-30 cells in each case. The histogram plot (see Supplementary Figure S2) was then fitted to an exponential function in order to find mean angular velocity (Figure 4C inset). The mean angular velocity was calculated by taking the half-life of the exponential (mean = $\lambda \ln 2$). Figure 4D shows the mean angular velocity (mean angle change per minute) for the nuclei of cells patterned on various shapes as well as on non-patterned random shapes. The rotation is found to be faster in case of unrestricted (non-patterned) random shaped cells (Imaged while ~70% confluent). For cells confined to geometrical shapes with varying rotational symmetry, we find that the circular cells rotate faster as compared to the triangular cells, while the square ones lying in between. The results clearly indicate that the cytoskeletal components are involved in and affect the nuclear dynamics. To investigate the effect of cell shape further, we seeded the cells on rectangle of varying aspect ratio, thus giving cells more stringent confinement in terms of translational motion as described in the next section.

Decreasing translational symmetry affects the nuclei shape as well as their propensity to rotate

In the previous section, we find that the rotationally symmetric cell shapes affect the nuclear rotation. When the cells are imposed with yet another geometrical confinement that is, a decrease in their translational symmetry, the cytoskeletal organization is no more rotationally symmetric. Increasing the aspect ratio of the rectangle imposes more stringent microenvironment around the nuclei. The translational trajectories of the nuclei inside the cells gets more and more confined in one direction as shown in Figure 5A (first row panel). Displacements in the other (confined) direction narrows down (second row panel). Since the nucleus spans the cellular space, the distance it can traverse is relatively high in the case of high aspect ratio (third row panel).

Interestingly, there is a significant decrease in the propensity to rotate for the nuclei. Figure 5B shows how increasing aspect ratio for rectangular shaped cells having same spreading area leads to a drastic decrease in the fraction of cells with rotating nuclei. The fraction is almost same for rotationally symmetric shapes in which more than three quarters of the cells undergo significant nuclear rotation. However, for a rectangle having aspect ratio 1:2, the fraction decreases down to around 50%. The fraction of cells having rotating nucleus is less than even 10% when we increase the aspect ratio to 1:5. This shows that translational symmetry significantly aids to the nuclear-cytoskeletal connections to undergo dynamic fluctuations and consequently lead to nuclear rotation. If we consider rotation as a cytoskeleton-independent process, then even in such geometric shapes, the nuclei should have significant rotation. Thus, this result establishes that cytoskeletal components actively control the nuclear dynamics.

As shown in earlier experiments, we also find that increasing aspect ratio also affects the nuclear shape. The circularity of the nucleus decreases significantly as we go from the ratio 1:1 to 1:5 as shown in Figure 5C. Thus, it can be inferred that the nuclear rotation is facilitated by its shape (circularity factor) which in turn is governed by the cell shape. The result thus indicates that there must be some active forces around the nucleus that are capable of inducing rotation in more circular nuclei. In summary, the comparison of these parameters for rotationally symmetric and asymmetric shapes gives an impression that the cytoskeletal arrangement around the nucleus can alter its dynamics. Based on the previous works on nuclear rotation on cells imposed to external physical stresses, we speculated that this alteration can be either due to the active hydrodynamics of cytoskeletal structures or due to a motor driven process (involving dynein). We investigate further these possibilities by using inhibitor drugs to understand up to what extent these cytoskeletal components and motor proteins are involved in the dynamics.

Drug inhibition of motor proteins affect the rotation suggesting that nuclear rotation is actomyosin as well as dynein dependent phenomenon

In the previous section, it has already been shown that cell shapes affect the nuclear dynamics, specifically nuclear rotation because of the altered cytoskeletal microenvironment surrounding the cell. In order to understand which components play a role in this dynamics and their propensities, specific drug inhibitors were used on the patterned cells. In this set of experiments, patterned triangular cells were used. Because amongst the three symmetric shapes, nuclei in triangular cells show the least rotational speed, any further decrease in the value would indicate an effect of drug targeting a particular cytoskeletal or motor component. The drugs that were used are blebbistatin and EHNA. Effect of inhibition of motor proteins was investigated using the drugs Blebbistatin and Erythro-9-(2-hydroxy-3-nonyl) adenine (EHNA). Blebbistatin has been shown to be highly specific in myosin motor inhibitor (19). EHNA acts as a specific inhibitor of dynein (20-21). Although EHNA has been shown to be a dynein ATPase inhibitor

and has been used in cell types like glioma cells (22), we ensured successful treatment of NIH 3T3 fibroblasts with EHNA by immunofluorescence-staining to find that there is no or little change in the cytoskeletal morphology i.e., actin and microtubule. Also, EHNA was found to be significantly effective in inhibiting mitosis) which also suggests that EHNA should be acting as a dynein inhibitor in NIH3T3 fibroblasts as well.

To investigate the effect of drugs, cells were seeded on the triangular patterns. Once the cells were properly spread, the usual media was replaced by media with various concentrations of drugs in it. This was followed by incubation for half an hour. Phase contrast time lapse movies were captured and movies were analyzed in the same manner as mentioned in the previous sections. Analysis of the nuclear dynamics was done in the same way as described in earlier sections. The angle versus time plot for the nuclei of drug treated cells is shown in Figure 6A (first row panel). A comparison of curve groups with the non-treated triangular cells clearly indicates that the extent of rotation is decreased in case of Blebbistatin treated cells whereas the nuclei of EHNA treated cells still undergo long rotational motions. A detailed quantitative analysis is shown in Figure 6A (second row panel) where the distribution of instantaneous angular speed has been fitted with an exponential. Clearly, the $t_{1/2}$ value is reduced in both the cases as compared to the non-treated triangular cells.

The mean angular speed of the nuclei treated with various drugs was then calculated using the relation, mean = $\lambda \ln 2$ as shown in Figure 6B. Treatment with EHNA, which is a dynein inhibitor, results in slight decrease in the mean angular speed of rotation. These results together suggest that there is a contribution of dynein motors in the context of nuclear rotation which has also been shown in other literatures in wound healing assays and imposing shear force on the cells. When cells were treated with blebbistatin in order to inhibit myosin II, we found a significant decrease in the nuclear rotation. This suggests that the actomyosin contractility (sometimes referred as active cytoskeleton) is also involved in the process. When we over-expressed actin by transfecting the cells with Actin EGFP plasmid, the number nuclei undergoing rotation reduced significantly (data not shown). In this experiment, we also observed that nuclear shape was not circular as it is in normal non-transfected cells. Most of the nuclei were ellipsoidal and although there was a high actomyosin activity around the nucleus (described in next section), no significant rotation was observed in the cells. These results together with the effect of myosin inhibition, suggest that an active acto-myosin hydrodynamics may also be significantly involved in rotation.

DISCUSSION

Although Triangle (C_3), Square (C_4) and Circle (C_∞) are all symmetrical two dimensional shapes, yet the steric hindrance due to cytoskeletal components in nuclear movement is expected to be least in case of a circle and most in case of a triangle amongst the three (Figure 4A). Hence, if we consider an internal active hydrodynamics that is resulting in nuclear rotation, then the rotation will be relatively faster in the circular cells as compared to the triangular ones. It is also interesting to find that randomly shaped unconstrained cells, on which no symmetry is imposed, have the fastest rotating nuclei. This also indicates that imposing symmetry reduces the tendency of a nucleus to rotate. If the rotation is considered to be dynein driven (5, 16), the probability of fluctuations or imbalance in torque on the nucleus would be higher in case of asymmetric structure. Hence, nuclei of randomly shaped cells would have higher propensity to rotate. The result thus supports that there are two open possibilities for nuclear rotation. First, the presence

of an active hydrodynamics around the nucleus and second, a motor-driven process involving dynein and microtubule as speculated by some earlier observations. As shown in Figure 5D, the nuclear shape is also affected when we impose translational asymmetry. The less circular an object be, more should be the hindrance to rotation in an active hydrodynamic medium. Thus, this observation again supports that active hydrodynamics plays significantly in this process. However, as suggested in one of the recent articles (16), the centrosome distance from nucleus centroid is crucial in defining the extent of rotation. We speculate that confining the cell in one direction will eventually lead an apparent decrease in the nuclear centroid-centrosome distance and hence the trend is expected. The comparison of various statistical parameters like statistics on run lengths and run times for the rotationally symmetric shapes should suggest more about the cytoskeletal arrangement around the nucleus and how it can alter its dynamics.

The results for inhibitory drugs (Figure 6B) indicate that the role played by molecular motor protein dynein is sufficient but not exclusive for nuclear rotation. Inhibitory action of EHNA is consistent with earlier experiments, in which the role of dynein motors in rotating the nucleus has been shown. However, comparing the extent of reduction in angular speed with that for myosin inhibitor, it seems that along with the proposed 'torque mechanism' for dynein, there are certainly other factors actively involved in such nuclear dynamics. Dynein is involved in cargo transport and is a minus-end directed motor. In a few models proposed for nuclear rotation, it has been speculated that the dynein molecules running through the microtubules near the nuclear envelope bind to the nucleus through their cargo binding domain. Any fluctuation in concentration of dynein on the two sides of centrosome will lead to a net torque. This torque has been shown to be sufficient for nuclear rotation. We find that myosin II inhibition also affects the propensity of rotation to a large extent. However, myosin molecules cannot be speculated for any similar mechanism as that for dynein because of their very small size and their existence as dimers creating tensile force in actin filaments. Its inhibition might lead to relieve from the tensile load for the nucleus employed by the actin filaments. Since the pre-stressed nucleus is already a balance of the tensile load by actin and a compressive load from microtubules, one of the possibilities may be that the microtubule-nuclear envelope connections become more stable and there is an over increased compressive load on nucleus. The fluctuating dynein concentration may not be sufficient to produce a torque that can counter the friction due to the increased compressive load. The other possibility is that more stable microtubule-nuclear connections will consequently affect the hydrodynamic activity of microtubules. Hence, the rotation is very little.

Recent theoretical advancements in the field of cellular mechanics, more specifically cytoskeletal mechanics suggest that the force generated by the molecular motors can strongly affect the cellular mechanics. The transient contractile stresses (in case of actomyosin) can drive the cytoskeletal networks out of equilibrium (23-25). The model concludes that such kinetics enhances the low frequency stress fluctuations and consequently leads to non-equilibrium diffusive motion within an elastic network. In yet another theoretical construction, the transient polymerization-depolymerization process itself is shown to be capable of bringing a force imbalance resulting in a net torque around the nucleus. Recent experiments on cytoplasmic microrheology have shown the mechanical architecture of adherent cells is biphasic- stiff contractile stress fibers and soft actin meshwork (26). We also observe the two distinct features in live cells (data not shown). Theoretical reconstructions suggest that non-thermal forces driven by myosin II is capable of inducing large non-equilibrium fluctuations. We have shown in this

work that inhibiting myosin II indeed affects nuclear dynamics drastically suggesting that the active actomyosin forces are involved in the nuclear rotation.

CONCLUSION

Although the dynamics of nucleus inside a stationary cell is regulated by many components including cytoskeleton as well as motor proteins, our current work suggests that cell shapes significantly affect this dynamics. Decrease in translational symmetry in two dimensions results in a drastic decrease in nuclei undergoing rotation and the dynamics is almost only translational. Moreover, the rotational symmetry of a cell also governs the nuclear rotation and we find that more the rotational symmetry, faster is the rotation in a cell. We further find out that the actomyosin plays a more significant role in rotation as compared to the dynein-microtubule system. Based on these results, we suggest that an active hydrodynamics involving actomyosin might be the main cause of nuclear rotation along with translocation in a stationary cell. We further would like to establish that such dynamics is possible because of the transient coupling between the actin cytoskeleton and the nuclear envelope. Nuclear rotation has been implicated to play vital role in chromosome orientation and segregation during mitosis. Further it might also be one of the mechanisms for mechanotransduction which has been shown to be crucial for gene regulation. This work can be extended to explore the biological significance of this slow dynamics of nuclear rotation in diffusion of various cytoplasmic molecules and movement of organelles, import and export mechanism for some of the transcription factor in/from the nucleoplasm. This might give an insight in mechanism of gene regulation in eukaryotic cells.

REFERENCES

1. Starr, D. A. 2007. Communication between the cytoskeleton and the nuclear envelope to position the nucleus. Mol Biosyst 3:583-589.
2. Hagan, I., and M. Yanagida. 1997. Evidence for cell cycle-specific, spindle pole body-mediated, nuclear positioning in the fission yeast Schizosaccharomyces pombe. J Cell Sci 110 (Pt 16):1851-1866.
3. Ingber, D. E. 2003. Tensegrity I. Cell structure and hierarchical systems biology. J Cell Sci 116:1157-1173.
4. Ingber, D. E. 2003. Tensegrity II. How structural networks influence cellular information processing networks. J Cell Sci 116:1397-1408.
5. Levy, J. R., and E. L. Holzbaur. 2008. Dynein drives nuclear rotation during forward progression of motile fibroblasts. J Cell Sci 121:3187-3195.
6. Pouthas, F., P. Girard, V. Lecaudey, T. B. Ly, D. Gilmour, C. Boulin, R. Pepperkok, and E. G. Reynaud. 2008. In migrating cells, the Golgi complex and the position of the centrosome depend on geometrical constraints of the substratum. J Cell Sci 121:2406-2414.
7. Reinsch, S., and P. Gonczy. 1998. Mechanisms of nuclear positioning. J Cell Sci 111 (Pt 16):2283-2295.
8. Luxton, G. W., E. R. Gomes, E. S. Folker, E. Vintinner, and G. G. Gundersen. 2010. Linear arrays of nuclear envelope proteins harness retrograde actin flow for nuclear movement. Science 329:956-959.
9. Lee, J. S., M. I. Chang, Y. Tseng, and D. Wirtz. 2005. Cdc42 mediates nucleus movement and MTOC polarization in Swiss 3T3 fibroblasts under mechanical shear stress. Mol Biol Cell 16:871-880.
10. Brosig, M., J. Ferralli, L. Gelman, M. Chiquet, and R. Chiquet-Ehrismann. 2010. Interfering with the connection between the nucleus and the cytoskeleton affects nuclear rotation, mechanotransduction and myogenesis. Int J Biochem Cell Biol 42:1717-1728.
11. Starr, D. A. 2009. A nuclear-envelope bridge positions nuclei and moves chromosomes. J Cell Sci 122:577-586.
12. Crisp, M., Q. Liu, K. Roux, J. B. Rattner, C. Shanahan, B. Burke, P. D. Stahl, and D. Hodzic. 2006. Coupling of the nucleus and cytoplasm: role of the LINC complex. J Cell Biol 172:41-53.
13. Haque, F., D. J. Lloyd, D. T. Smallwood, C. L. Dent, C. M. Shanahan, A. M. Fry, R. C. Trembath, and S. Shackleton. 2006. SUN1 interacts with nuclear lamin A and cytoplasmic nesprins to provide a physical connection between the nuclear lamina and the cytoskeleton. Mol Cell Biol 26:3738-3751.
14. King, M. C., T. G. Drivas, and G. Blobel. 2008. A network of nuclear envelope membrane proteins linking centromeres to microtubules. Cell 134:427-438.
15. Mazumder, A., and G. V. Shivashankar. 2010. Emergence of a prestressed eukaryotic nucleus during cellular differentiation and development. J R Soc Interface 7 Suppl 3:S321-330.
16. Wu, J., K. C. Lee, R. B. Dickinson, and T. P. Lele. 2010. How dynein and microtubules rotate the nucleus. Journal of Cellular Physiology.
17. Tabaliov, N. A., and D. M. Svirachev. 2007. Plasma-chemical model, describing the surface treatment of polymers in RF-discharge. Appl Surf Sci 253:4242-4248.

18. Svirachev, D. M., and N. A. Tabaliov. 2006. Treatment of polymer surfaces in plasma Part II. Qualitative analysis. J Phys Conf Ser 44:158-161
19. Kovacs, M., J. Toth, C. Hetenyi, A. Malnasi-Csizmadia, and J. R. Sellers. 2004. Mechanism of blebbistatin inhibition of myosin II. J Biol Chem 279:35557-35563.
20. Penningroth, S. M., A. Cheung, P. Bouchard, C. Gagnon, and C. W. Bardin. 1982. Dynein ATPase is inhibited selectively in vitro by erythro-9-[3-2-(hydroxynonyl)]adenine. Biochem Biophys Res Commun 104:234-240.
21. Forman, D. S., K. J. Brown, and M. E. Promersberger. 1983. Selective inhibition of retrograde axonal transport by erythro-9-[3-(2-hydroxynonyl)]adenine. Brain Res 272:194-197.
22. Yamamoto, M., S. O. Suzuki, and M. Himeno. 2010. The effects of dynein inhibition on the autophagic pathway in glioma cells. Neuropathology 30:1-6.
23. MacKintosh, F. C., and A. J. Levine. 2008. Nonequilibrium mechanics and dynamics of motor-activated gels. Phys Rev Lett 100:018104.
24. Lau, A. W., B. D. Hoffman, A. Davies, J. C. Crocker, and T. C. Lubensky. 2003. Microrheology, stress fluctuations, and active behavior of living cells. Phys Rev Lett 91:198101.
25. Levine, A. J., and F. C. MacKintosh. 2009. The mechanics and fluctuation spectrum of active gels. J Phys Chem B 113:3820-3830.
26. Hale, C. M., S. X. Sun, and D. Wirtz. 2009. Resolving the role of actoymyosin contractility in cell microrheology. PLoS One 4:e7054.

FIGURE LEGENDS

Figure 1

Standardization of micro-contact printing of labeled fibronectin: A. Examples of over-dried stamping B. Examples of patterns transferred properly but stamped improperly C. an example of stamping transferred and stamped properly. D. Intensity profile of a line drawn across the micro-pattern of Figure 1C.

Figure 2

Optimization of cell seeding on the micro-patterns: A. Example of cells seeded and properly spread on the patterns B. Multiple cells on the same pattern C. Plot showing percentage of single cells on the pattern as a function of cell density.

Figure 3

Analysis of nuclear dynamics: A. Typical trajectories for a symmetric triangular (black) and an asymmetric 1:5 shape (white) B. Two dark spots for tracking the time lapse movie (the mean position and rotation angle determined by the formula given) C. Resolving the trajectory into rotational and translational component

Figure 4

Analysis of the rotational component: A. time lapse of a typical fibroblast cell on triangular pattern. Arrow marks a dark spot which changes the position during rotation. B. Angle versus time plot. Labels characterize the curve into rotation, reversal and stalling C. Comparison of mean angular speed for all three geometries and random shaped cells D. Angle trajectory plots and method for calculation of mean angular speed.

Figure 5

Analysis of dynamics of cells on patterns of different aspect ratios: A. x-y plots and trajectories of nuclei on cell shapes of different aspect ratios B. A comparison of percentage of rotating cells on various geometric shapes C. A comparison of nuclear circularity of cells patterned on various geometries.

Figure 6

Effect of inhibitor drugs on rotation: A. i. Angle versus time plots for cells treated with blebbistatin and EHNA ii. Exponential curve fitting for the instantaneous angular speed distribution for both drugs. C. Comparison of mean angular velocity of non-treated cells with triangular cells treated with inhibitor drugs.

Figure 1

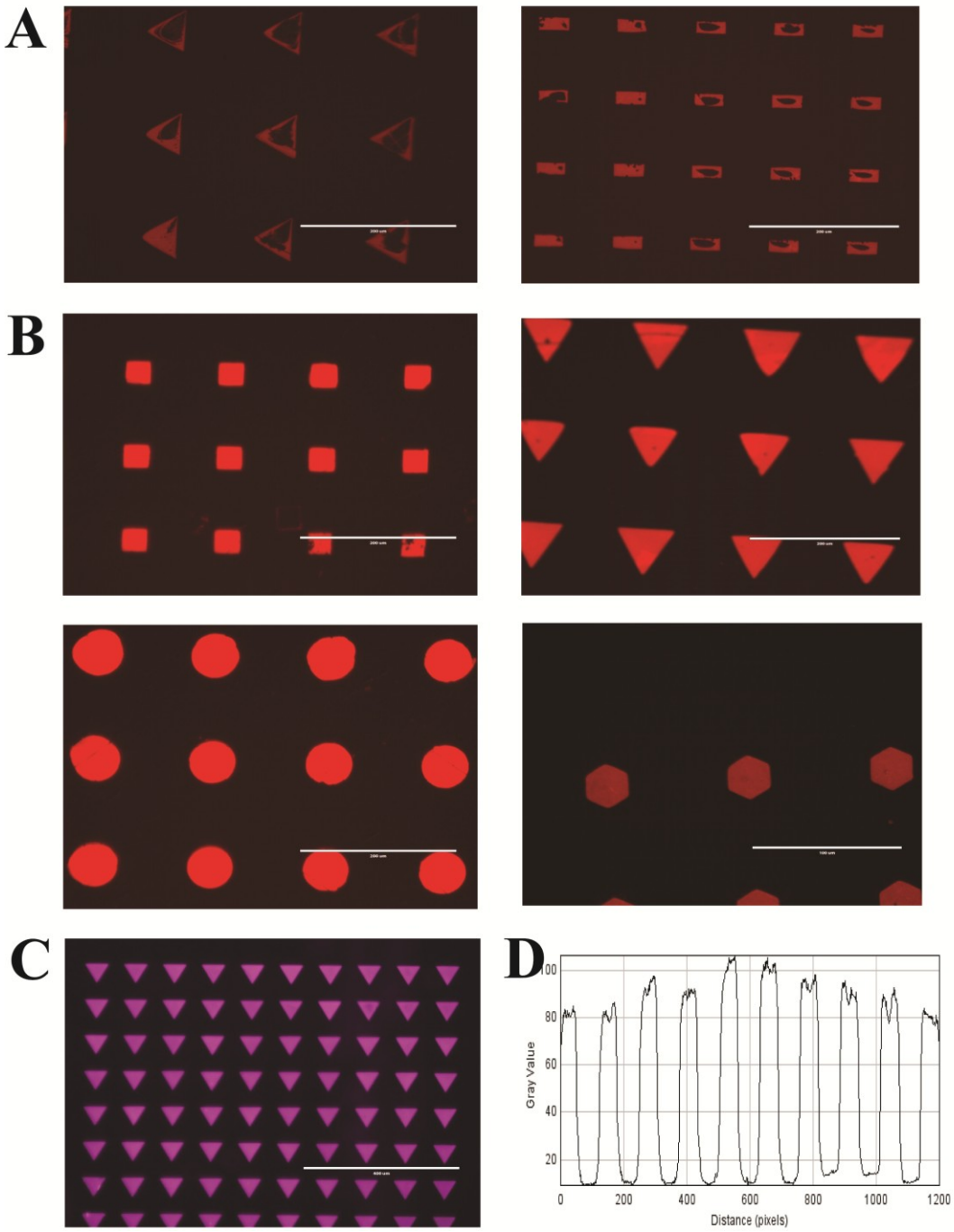
A
B
C
D
Gray Value
Distance (pixels)
0
200
400
600
800
1000
1200
20
40
60
80
100

Figure 2

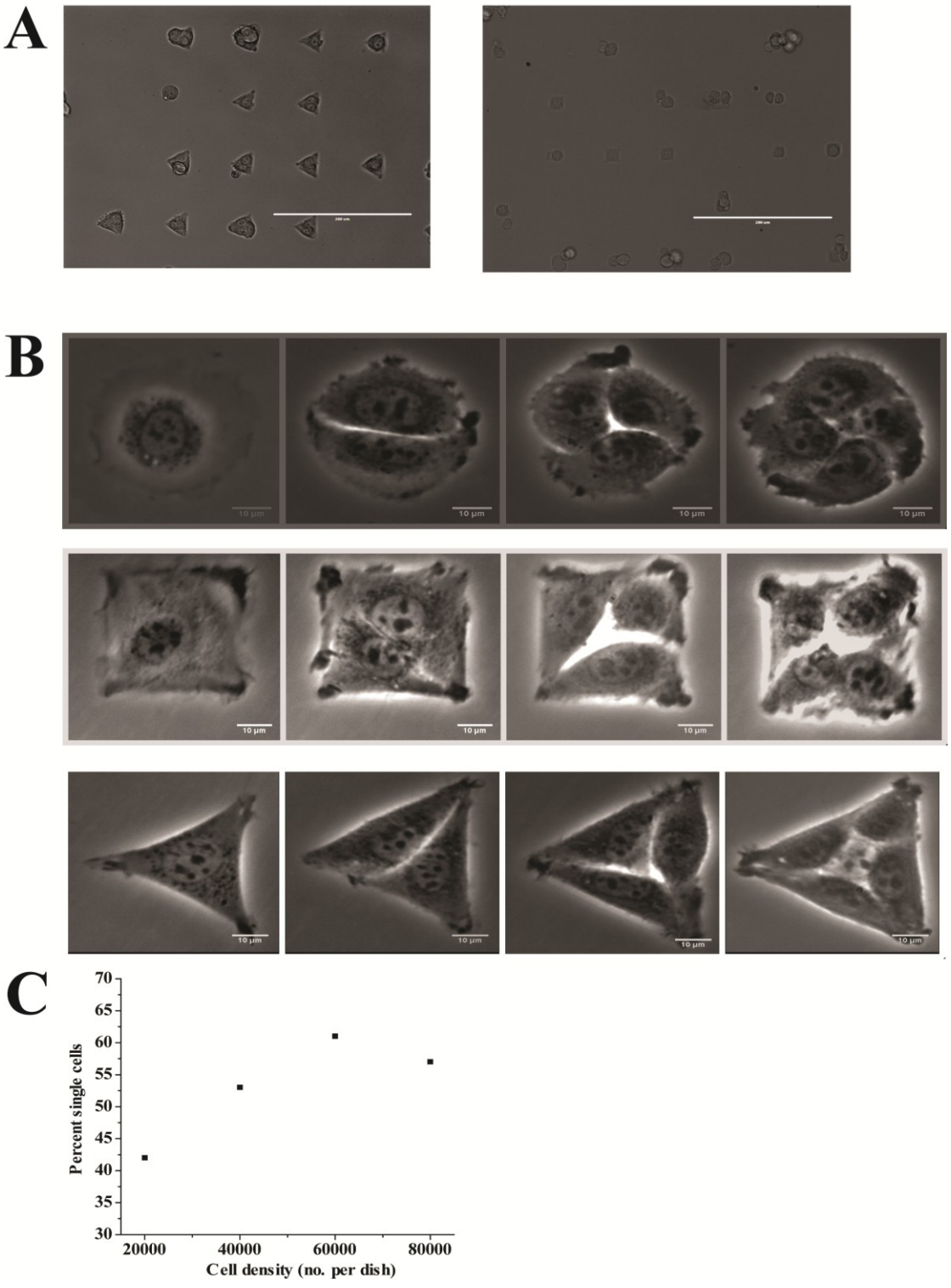
A
B
C
Percent single cells
70
65
60
55
50
45
40
35
30
20000
40000
60000
80000
Cell density (no. per dish)

Figure 3

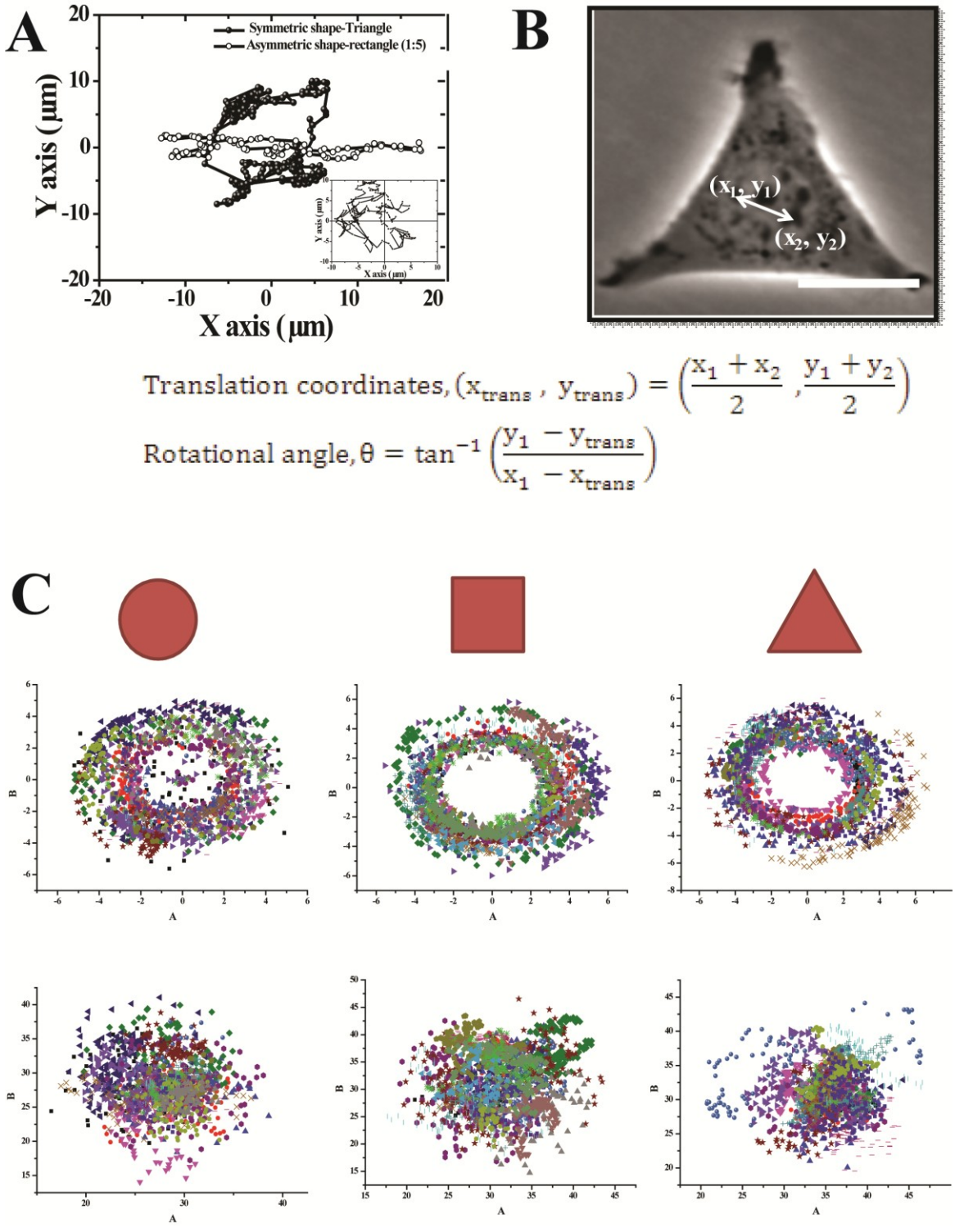
A
Symmetric shape-Triangle
Asymmetric shape-rectangle (1:5)
Y axis (μm)
X axis (μm)
B
(x_1, y_1)
(x_2, y_2)
Translation coordinates, $(x_{trans}, y_{trans}) = \left(\frac{x_1 + x_2}{2}, \frac{y_1 + y_2}{2}\right)$
Rotational angle, $\theta = \tan^{-1}\left(\frac{y_1 - y_{trans}}{x_1 - x_{trans}}\right)$
C
A
B

Figure 4

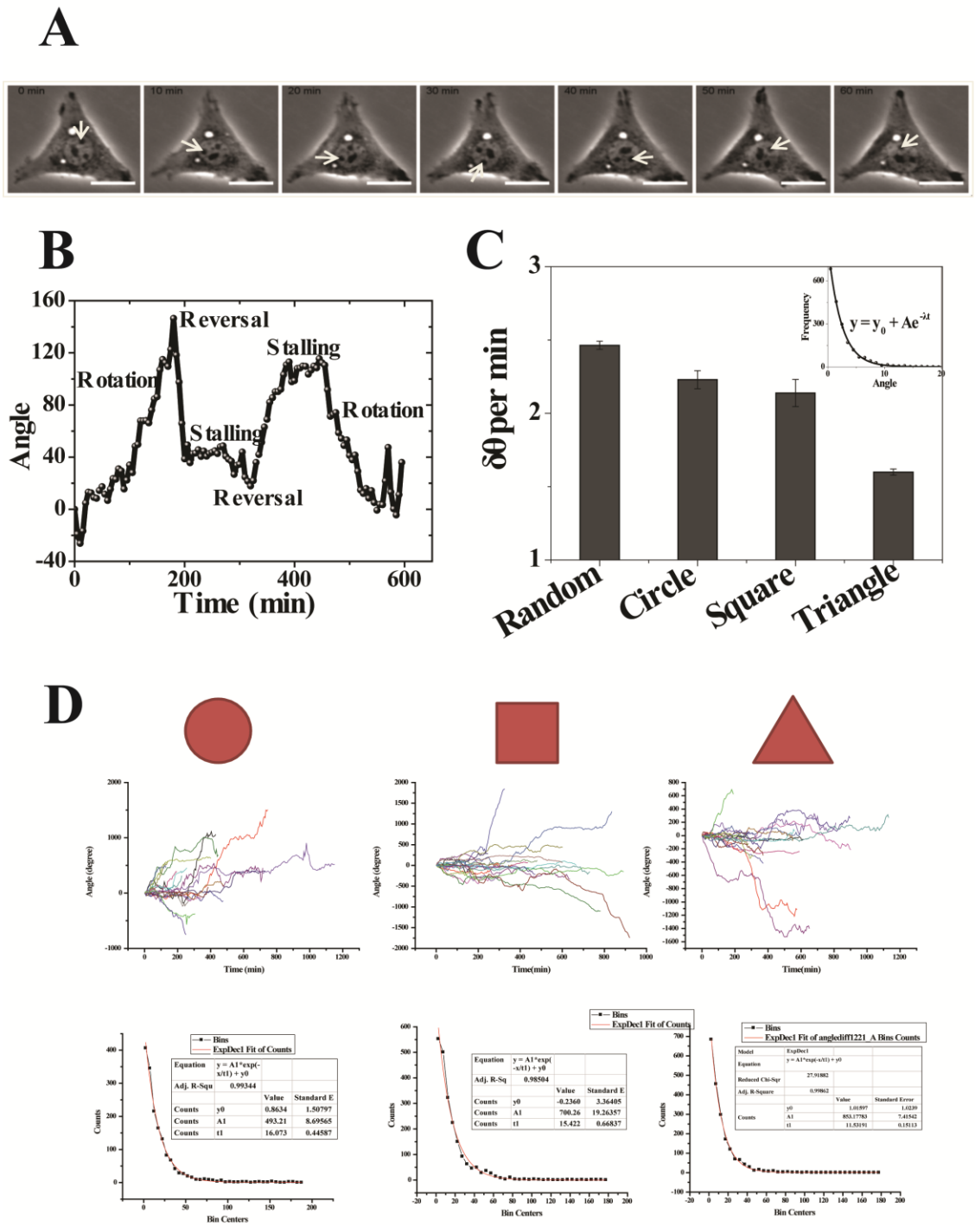
A
0 min
10 min
20 min
30 min
40 min
50 min
60 min
B
Reversal
Stalling
Rotation
Stalling
Rotation
Reversal
Angle
Time (min)
C
δθ per min
Random
Circle
Square
Triangle
Frequency
Angle
D
Angle (degree)
Time (min)
Time(min)
Bins
ExpDec1 Fit of Counts
Counts
Bin Centers

Figure 5

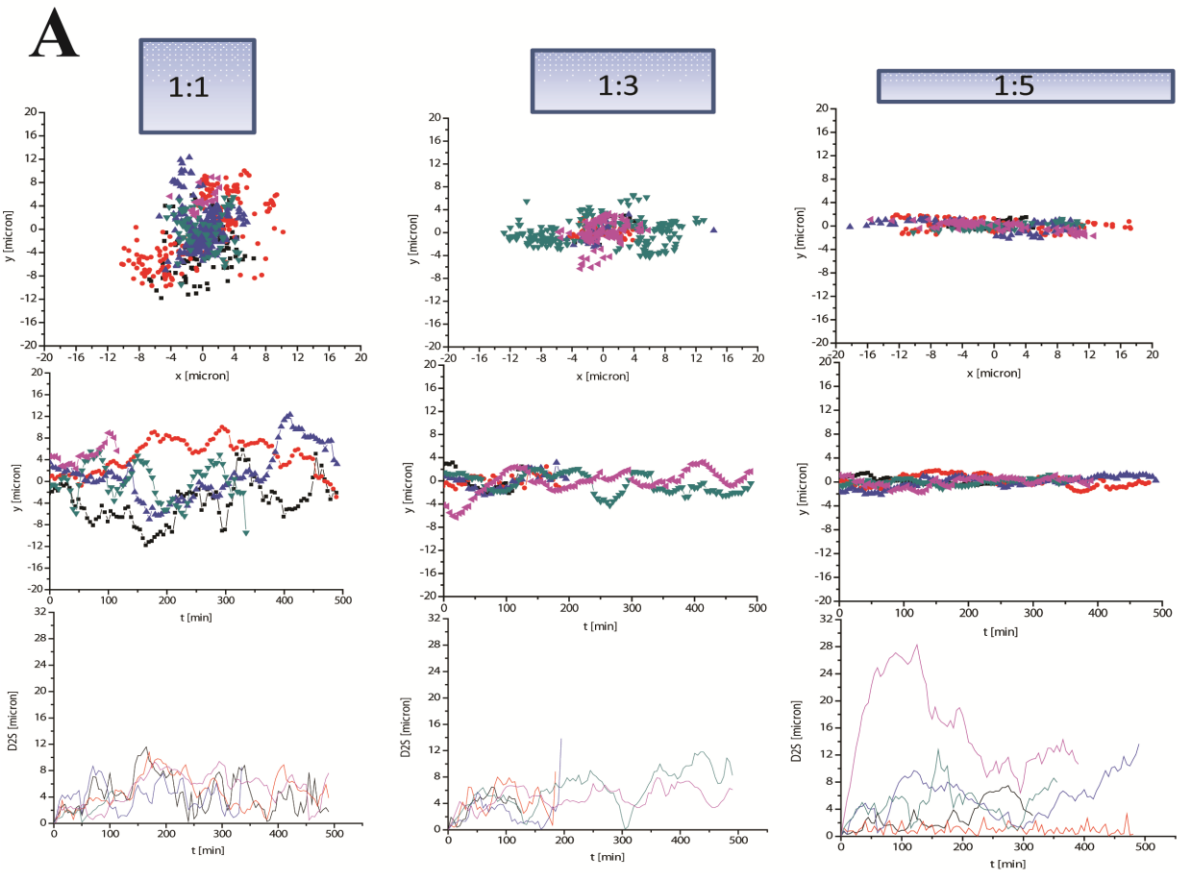
A
1:1
1:3
1:5
x [micron]
y [micron]
t [min]
D2S [micron]

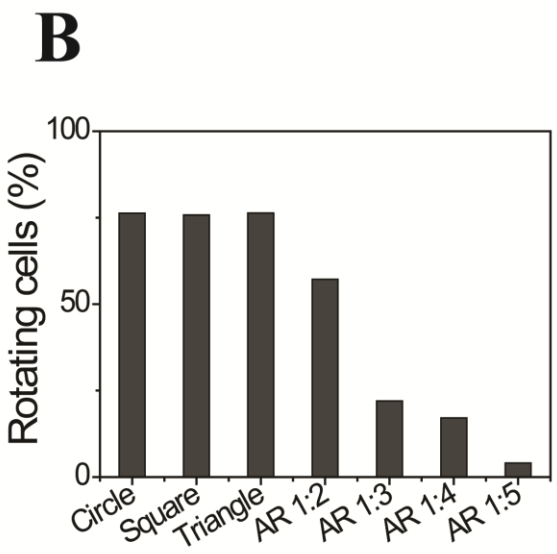
B
Rotating cells (%)
100
50
0
Circle
Square
Triangle
AR 1:2
AR 1:3
AR 1:4
AR 1:5

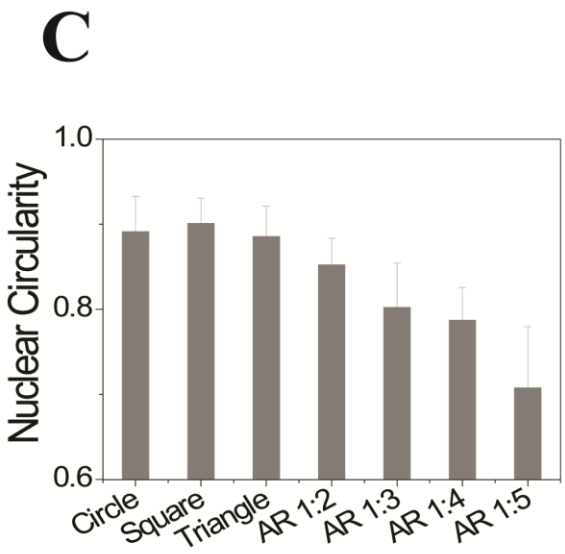
C
Nuclear Circularity
1.0
0.8
0.6
Circle
Square
Triangle
AR 1:2
AR 1:3
AR 1:4
AR 1:5

Figure 6

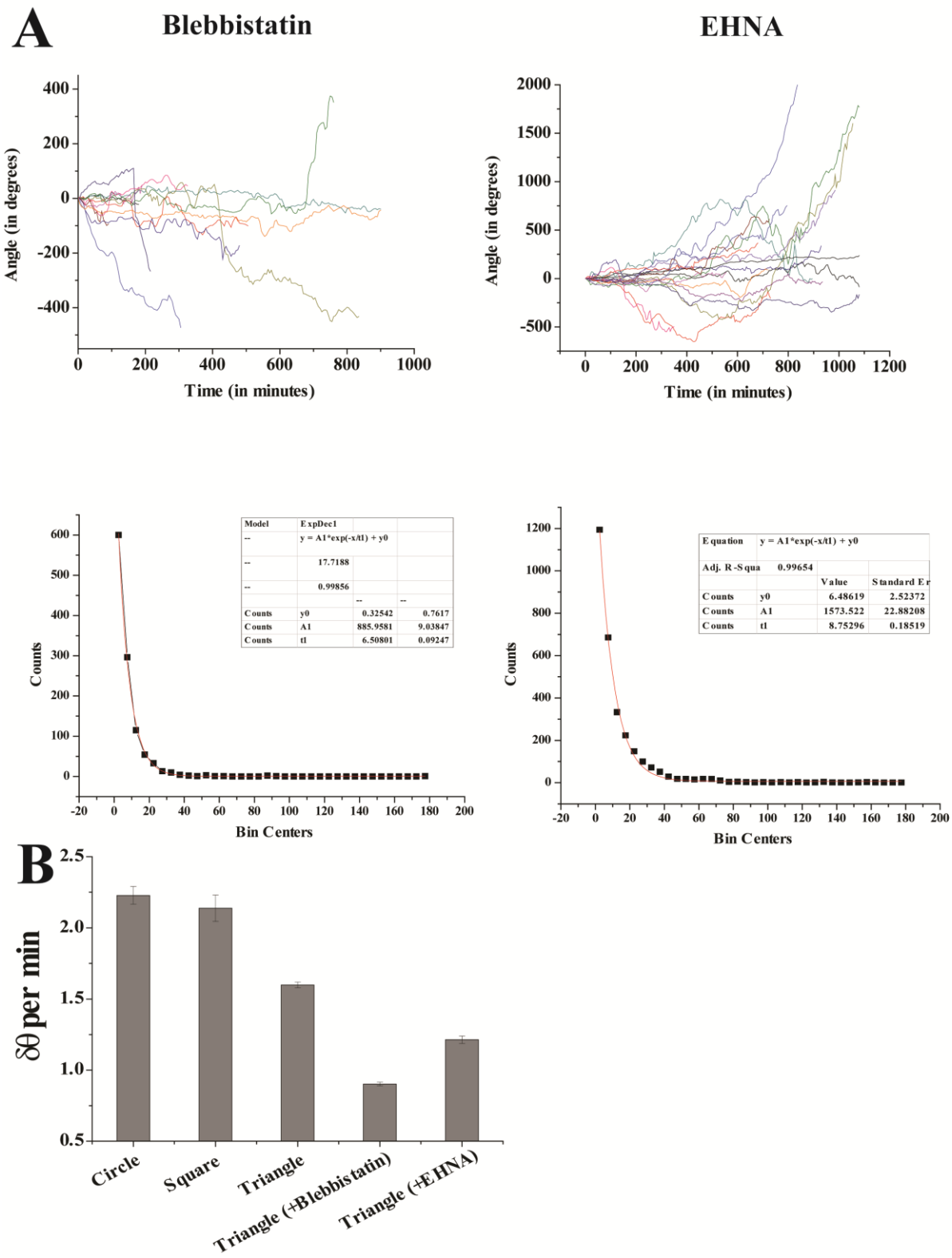
A
Blebbistatin
EHNA
Angle (in degrees)
Time (in minutes)
Counts
Bin Centers
Model ExpDec1
y = A1*exp(-x/t1) + y0
17.7188
0.99856
Counts y0 0.32542 0.7617
Counts A1 885.9581 9.03847
Counts t1 6.50801 0.09247
Equation y = A1*exp(-x/t1) + y0
Adj. R-Squa 0.99654
Value Standard Er
Counts y0 6.48619 2.52372
Counts A1 1573.522 22.88208
Counts t1 8.75296 0.18519
B
δθ per min
Circle
Square
Triangle
Triangle (+Blebbistatin)
Triangle (+EHNA)

Supplementary Material

Impact of Cellular Geometry on Nuclear Dynamics

Madhuresh Sumit[1] & G V Shivashankar[2]

[1]Indian Institute of Science Education and Research, Homi Bhabha Road, Pashan, Pune 411008, India

[2]Mechanobiology Institute and Department of Biological Sciences, Science Drive 4, National University of Singapore, Singapore

Figure S1

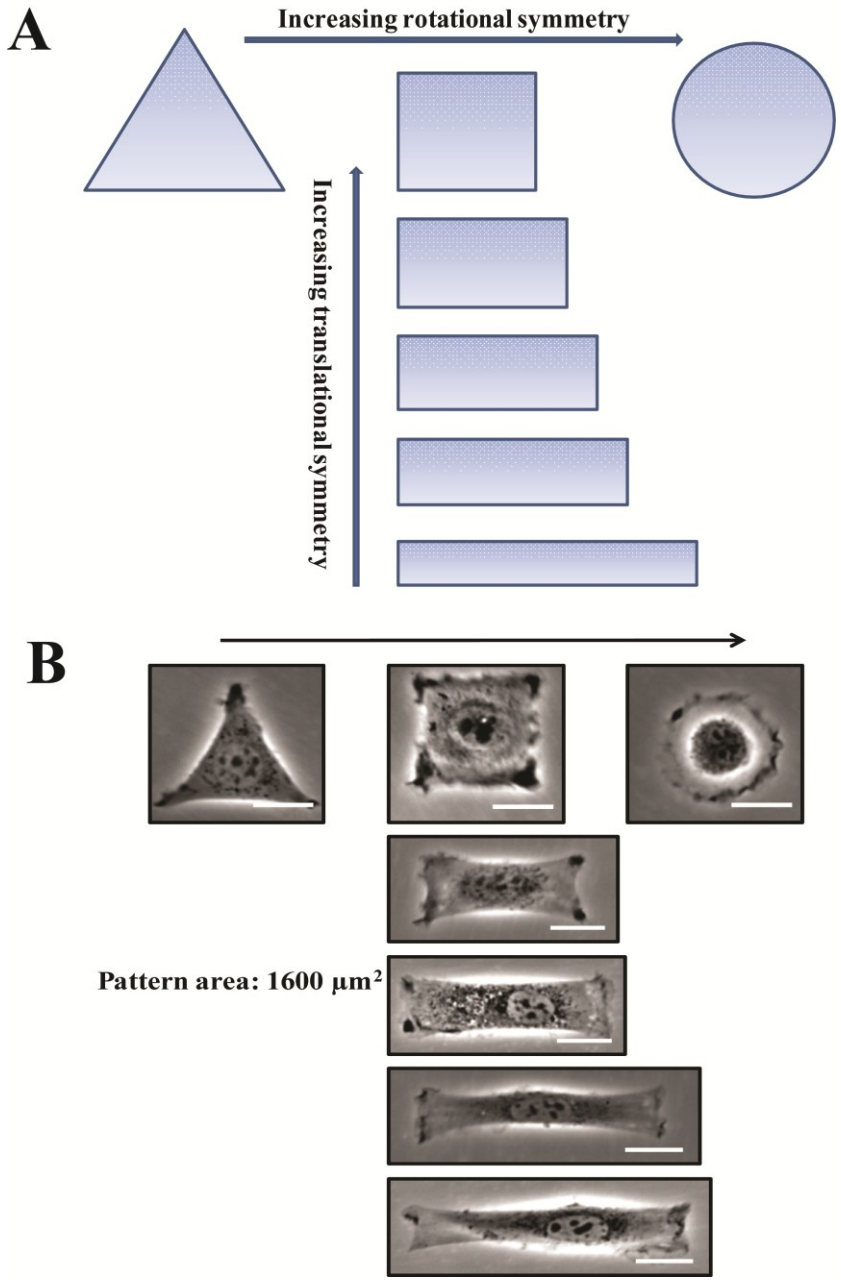

Experimental Scheme: A. Schematic diagram for increasing rotational and translational symmetry B. cells spread on the micro-patterns of various geometries as shown in Figure 3'A (pattern area 1600 μm^2)

Figure S2

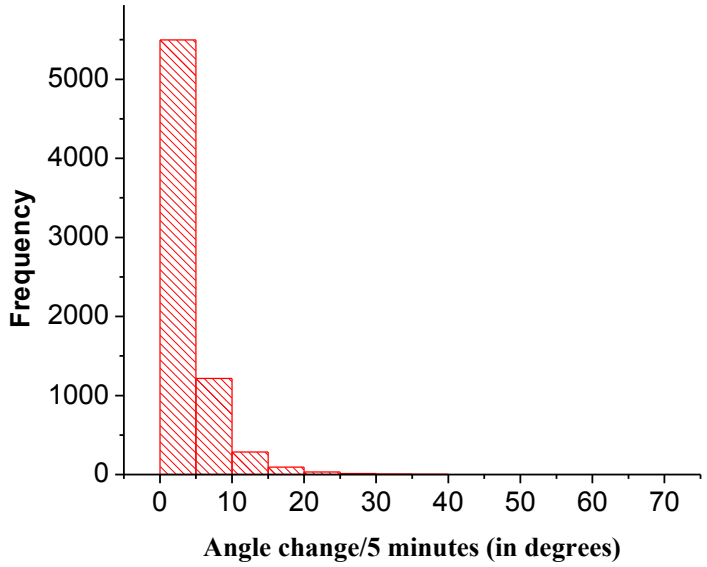

Figure S2: Histogram plot for angle change (per 5 minutes). The histogram is then fitted with an exponential decay function in order to find the $t_{1/2}$.

Figure S3

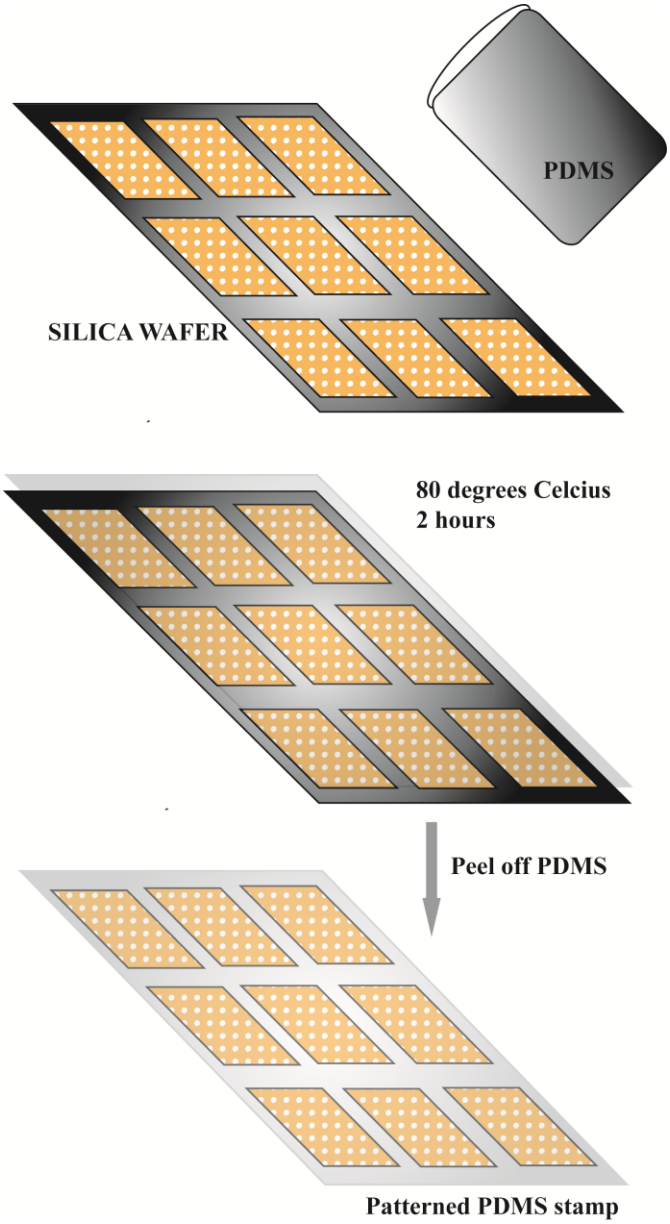

Figure S3
Illustration of PDMS stamp casting protocol: Step1- PDMS (mixed with cross-linker in the ratio 10:1) is poured on clean silica wafer. Step 2- The PDMS is cured at 80 degree Celsius for around 2 hours. Step 3- The stamp is peeled off from the wafer and used for micro-contact printing.